ELSEVIER

Volume 182, Number 5, May 2009

JOURNAL OF SOLID STATE CHEMISTRY

www.elsevier.com/locate/jssc

CONTENTS

Abstracted/indexed in BioEngineering Abstracts, Chemical Abstracts, Coal Abstracts, Current Contents/Physics, Chemical, & Earth Sciences, Engineering Index, Research Alert, SCISEARCH, Science Abstracts, and Science Citation Index. Also covered in the abstract and citation database SCOPUS®. Full text available on ScienceDirect®.

Regular Articles

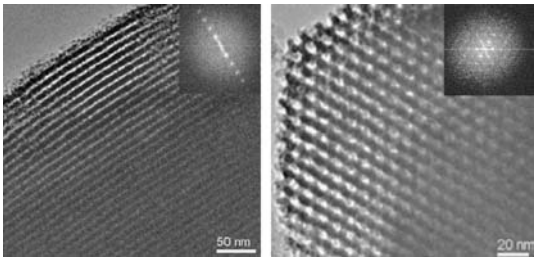

TEM images of the calcined mesoporous catalyst MSC_x ($x=1.1$), in which no aggregated ZrO_2 particles can be observed. The corresponding electron diffraction (insets in figures) indicated the final product was a mesoporous material with a crystalline framework.

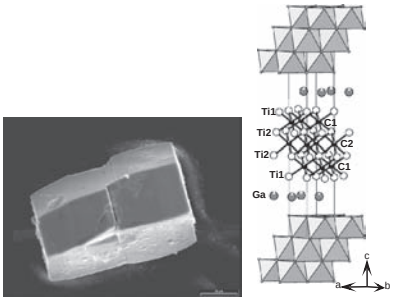

Single crystals of Ga-containing MAX-Phases $(TiC)_n(TiGa)$ ($n=1, 3$) were grown from a metallic melt including and characterised by X-ray diffraction. Ti_4GaC_3 is one of the few 413-phase and the first containing Ga.

Regular Articles—Continued

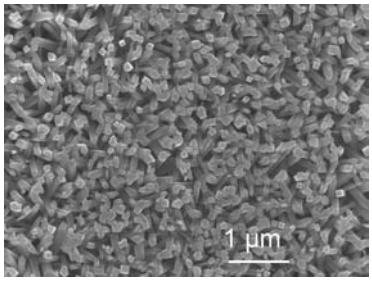

The rutile film consisting of rectangular nanorods is successfully deposited on glass substrate in presence of ionic liquid (IL) of [Bmim]Br. The nanorods were rectangular with width of 100–200 nm and length of more than 1 μm, which grew up typically along c-axis to form the arrays against the substrate.

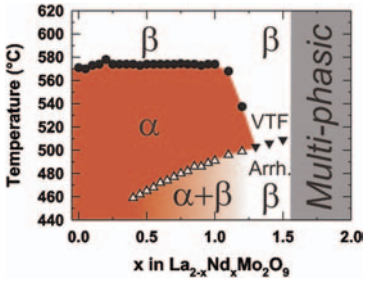

Metastable–stable phase diagram of the solid solution $La_{2-x}Nd_xMo_2O_9$ determined from DTA. The topological metastability of the high-temperature cubic β-form which goes back to monoclinic stable α-form above 450–500 °C is shown in the intermediate range $0.4 \leqslant x \leqslant 1.2$. Above $x=1.2$, this transition progressively changes into a thermal trace of the postulated Arrhenius/VTF transformation of transport mechanism.

Continued

Synthesis, structure, and magnetic and electronic properties of $Cs_2Hg_2USe_5$
Daniel E. Bugaris, Daniel M. Wells and James A. Ibers
Page 1017

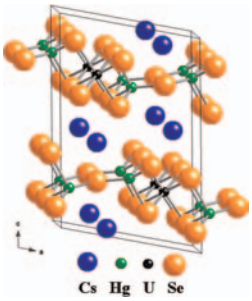

View of the crystal structure of $Cs_2Hg_2USe_5$.

A fast route to obtain manganese spinel nanoparticles by reduction of K-birnessite
F. Giovannelli, T. Chartier, C. Autret-Lambert, F. Delorme, M. Zaghrioui and A. Seron
Page 1021

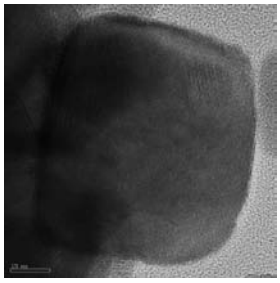

TEM image showing Mn_3O_4 particle after treatment of birnessite with an addition of hydrazine during 24 hours.

High temperature phase transition in SOFC anodes based on $Sr_2MgMoO_{6-\delta}$
D. Marrero-López, J. Peña-Martínez, J.C. Ruiz-Morales, M.C. Martín-Sedeño and P. Núñez
Page 1027

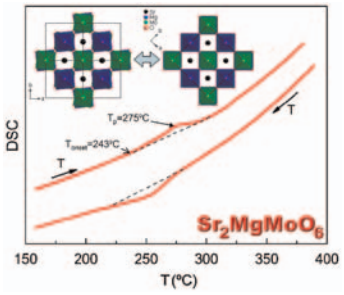

The double perovskite Sr_2MgMoO_6, recently proposed as an efficient SOFC anode for direct hydrocarbon oxidation, exhibits a reversible structural phase transition from triclinic to cubic at 275 °C.

Synthesis, crystal structure, and electrical and magnetic properties of Ce_3MoO_7
Philippe Gall and Patrick Gougeon
Page 1035

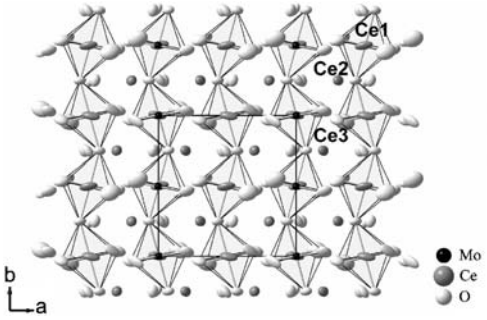

We report the synthesis, crystal structure, and electrical and magnetic properties of the novel compound Ce_3MoO_7 containing infinite chains of trans-corner-sharing MoO_6 octahedra.

Syntheses, structures and properties of a series of photochromic hybrids based on Keggin tungstophosphates
Li-Zhi Zhang, Wen Gu, Zhili Dong, Xin Liu, Bing Li and Mei-Ling Liu
Page 1040

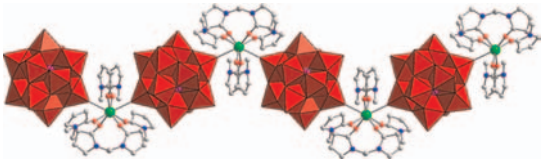

A series of photochromic hybrids based on Keggin tungstophosphates and lanthanides have been synthesized and characterized by elemental analysis, IR, UV–vis, and single-crystal X-ray diffraction. Their photochromic, magnetic, and luminescent properties have been studied.

Solvothermal synthesis and luminescent properties of monodisperse $LaPO_4$:*Ln* (*Ln* = Eu^{3+}, Ce^{3+}, Tb^{3+}) particles
Piaoping Yang, Zewei Quan, Chunxia Li, Zhiyao Hou, Wenxin Wang and Jun Lin
Page 1045

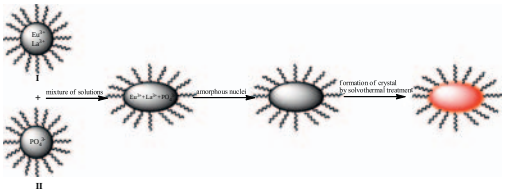

Monodisperse rare-earth ion (Eu^{3+}, Ce^{3+}, Tb^{3+}) doped $LaPO_4$ phosphors with monazite-type structure and uniform oval morphology and strong emission intensity have been prepared through a facile solvothermal process.

Cobalt oxide hollow microspheres with micro- and nano-scale composite structure: Fabrication and electrochemical performance

Feifei Tao, Cuiling Gao, Zhenhai Wen, Qiang Wang, Jinghong Li and Zheng Xu

Page 1055

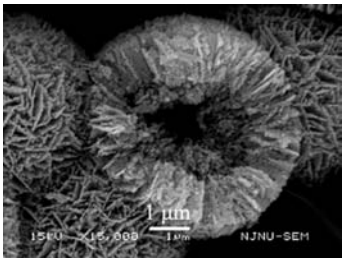

Co_3O_4 hollow microspheres self-assembled by nanosheets are successfully fabricated by a template-free wet-chemical approach. The hollow microspheres are in good morphology purity and homogeneous size. Co_3O_4 hollow microspheres constructed by porous nanosheets show the high discharge capacity of 1048 mAh g^{-1}, indicating it to be the potential electrode material of Li-ion battery.

Sonochemical fabrication of fluorinated mesoporous titanium dioxide microspheres

Changlin Yu, Jimmy C. Yu and Mui Chan

Page 1061

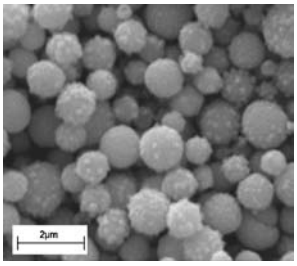

A novel method for preparing fluorinated mesoporous TiO_2 microspheres was developed by a combined ultrasonic and hydrothermal treatment. The fluorinated TiO_2 microspheres show high crystallinity, stability and enhanced photocatalytic activity.

Precipitation synthesis of lanthanide hydroxynitrate anion exchange materials, $Ln_2(OH)_5NO_3 \cdot H_2O$ (Ln = Y, Eu–Er)

Sheena A. Hindocha, Laura J. McIntyre and Andrew M. Fogg

Page 1070

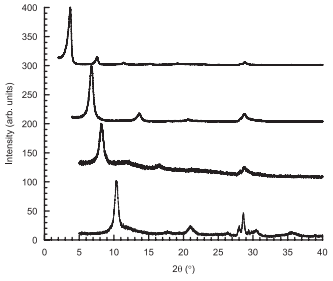

New anion exchangeable layered hydroxynitrates, $Ln_2(OH)_5NO_3 \cdot H_2O$ (Ln = Y, Eu - Er) have been synthesized via a precipitation route. These materials have been shown to be very flexible intercalation hosts undergoing facile exchange reactions with organic carboxylate and sulfonate anions.

Syntheses, structures, magnetism, and optical properties of gadolinium scandium chalcogenides

Geng Bang Jin, Eun Sang Choi and Thomas E. Albrecht-Schmitt

Page 1075

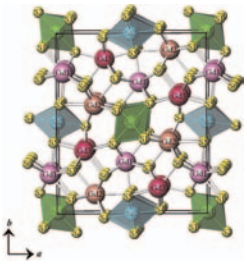

A view of the three-dimensional structure of $Gd_{3.04}Sc_{0.96}S_6$ along the c axis.

Formation of calcium carbonate films on chitosan substrates in the presence of polyacrylic acid

Linghao He, Rui Xue and Rui Song

Page 1082

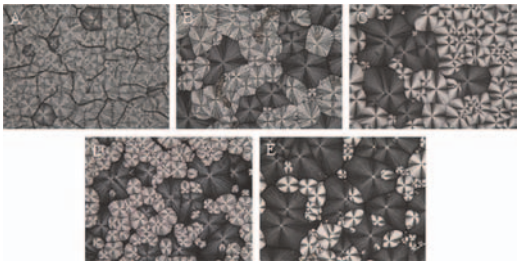

Chitosan membranes with different degrees of deacetylation (DA) are employed as support to culture calcium carbonate ($CaCO_3$). In high concentration of polyacrylic acid (PAA), the $CaCO_3$ films obtained consisted of vaterite. However, the $CaCO_3$ film grown on chitosan with 8% DA mainly consisted of vaterite as opposed to aragonite for chitosan with 8% DA.

CTAB-assisted synthesis and photocatalytic property of CuO hollow microspheres

Shunli Wang, Hui Xu, Liuqin Qian, Xi Jia, Junwei Wang, Yangyi Liu and Weihua Tang

Page 1088

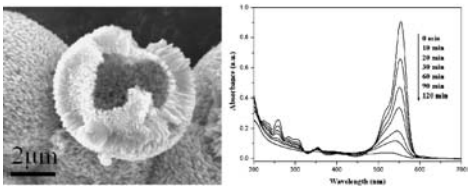

Dandelion-like CuO hollow microspheres were fabricated through a hydrothermal method. The prepared products exhibited a high photocatalytic activity for the photocatalytic decolorization of Rhodamine B aqueous solution under UV-light illumination.

Continued

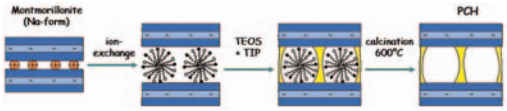

Synthesis of the montmorillonite based porous clay heterostructures (PCHs) intercalated with silica–titania pillars has been performed. The mechanism of the thermal degradation of organic templates in the pore system of PCHs was studied. PCHs were characterized with respect to structure, texture, composition, surface acidity, thermal stability and form of introduced titanium.

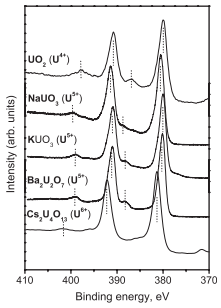

U4f X-ray photoelectron spectroscopy (XPS) spectra of $NaUO_3$, KUO_3 and $Ba_2U_2O_7$, indicating single valence state of uranium in these compounds. U4f XPS spectra of UO_2 (U^{4+}) and $Cs_2U_4O_{13}$ (U^{6+}) are shown for a comparison.

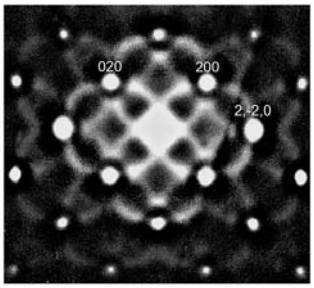

An 〈001〉 zone axis EDP typical of Li_4NbO_4F.

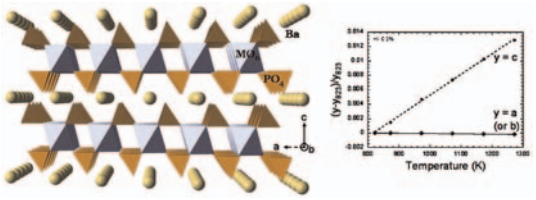

The layered high-temperature form of $BaM(PO_4)_2$, only expands along the c-axis.

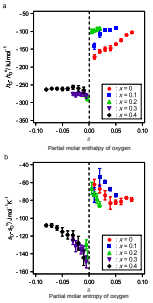

In order to elucidate the relation between thermodynamic quantities, the defect structure, and the defect equilibrium in $La_{2-x}Sr_xNiO_{4+\delta}$, statistics thermodynamic calculation is carried out and calculated results are compared to those obtained from experimental data.

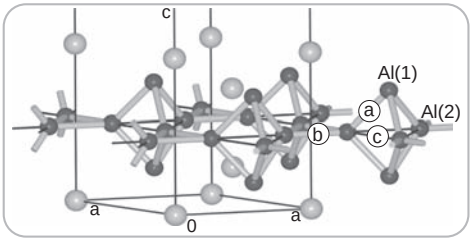

Al_5 layers of Kagomé nets in the new binary electron precise *Zintl* compound $Ba_{3.5}Al_5$, also found in Ba_3Al_5 and Ba_4Al_5.

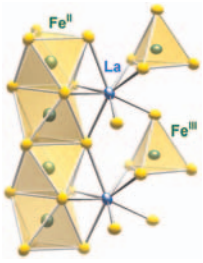

Rods of face-sharing $[Fe^{II}S_6]$-octahedra and $[Fe^{III}S_4]$-tetrahedra, all pointing in the same direction, dominate the polar structure. Vacancies in the octahedral Fe positions downgrade one-dimensional metallic conductivity to an activated semi-conducting behavior.

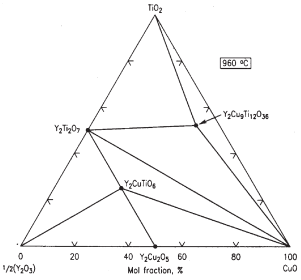

Phase diagram of the Y_2O_3–CuO–TiO_2 system prepared in air at 960 °C.

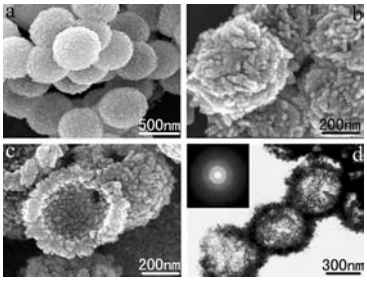

ZnO hollow spheres with porous shell were synthesized by a one-step polyoxometalate-assisted solvothermal route at low temperature. Room temperature photoluminescence spectrum of the ZnO hollow spheres exhibits exciting emission features with a broad band covering nearly all the visible region.

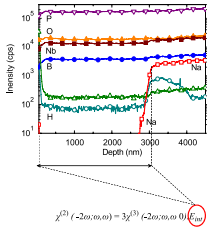

The sodium to barium substitution strongly influences the space charge implementation (E_{int}) at the anode side of the poled glass and thus its nonlinear optical properties.

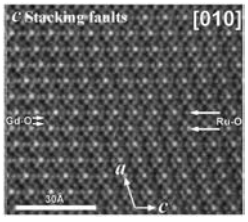

Single crystals of $Ln_5Ru_2O_{12}$ (*Ln* = Pr, Nd, Sm–Tb) were grown out of NaOH/KOH fluxes in sealed silver tubes. The crystal structure consists of one-dimensional chains of edge-sharing RuO_6 octahedral pairs along the *b* axis, separated by a two dimensional LnO_x polyhedral framework. Each RuO_6 octahedral pair is separated alternately by Ln atoms and its disordered component, observed as stacking faults in the HRTEM images.

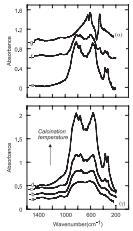

Infrared spectra of alumina sequence $\gamma \rightarrow \delta \rightarrow \theta \rightarrow \alpha$–$Al_2O_3$ obtained from 24h calcinations of boehmite at 873 K (a), 1123 K (b), 1223 K (c), 1273 K (d), 1293 K (e), 1383 K (f), 1573 K (g).

Continued

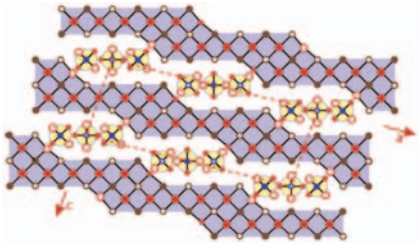

This work reports on the *ab initio* determination of $Bi_{10}Mo_3O_{24}$ structure, as well as its refinement by using the Rietveld method, from the combination of X-ray and neutron diffraction powder data. It belongs to the monoclinic system, space group $C2$, with cell parameters: $a=23.7282(2)$ Å, $b=5.64906(6)$ Å, $c=8.68173(9)$ Å, $\beta=95.8668(7)^\circ$ with $Z=2$.

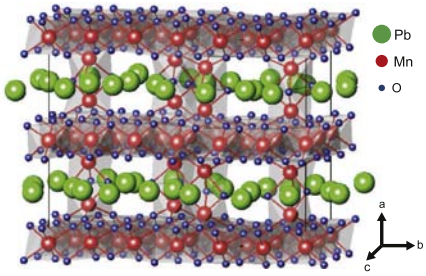

The crystal structure of $Pb_3Mn_7O_{15}$ has been reinvestigated by synchrotron powder diffraction. The compound crystallizes in the orthorhombic space group *Pnma* and shows no structural transition between 15 and 295 K.

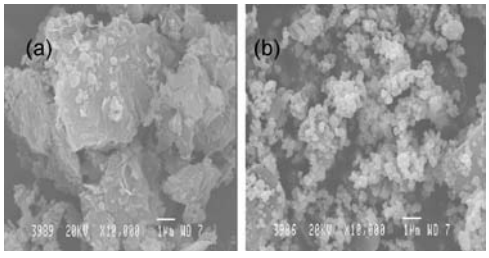

SEM image of (a) the Cu_2O–$Al(OH)_3$ composite obtained on reductive decomposition of $CuAl_4$-LDH and (b) Cu_2O obtained on leaching of $Al(OH)_3$ from (a).

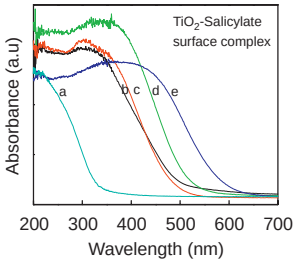

A new titania–salicylate nanostructure material has been synthesized, which exhibit a considerable red shift towards the visible region vis-à-vis nanocrystalline (organic-free) TiO_2 and blue luminescence at room temperature.

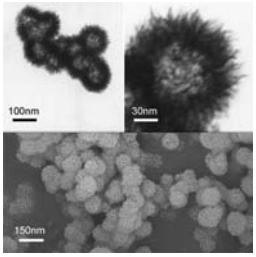

The mesoscale assembly of NiO nanosheets into spheres have been achieved by a solvothermal method. N_2 adsorption/desorption isotherms show the S_{BET} of NiO is tunable. NiO spheres show large discharge capacity and slow capacity-fading rate.

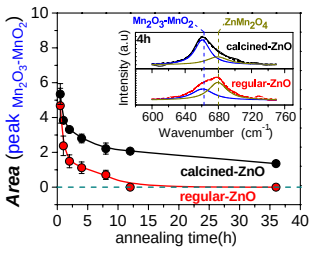

Recently new room temperature interphase magnetism has been reported to appear in ZnO–MnO_2 system. Raman spectroscopy is used to evidence both the nature of the interphase reaction and the kinetic. The interphase evolved towards complete formation of the spinel phase. The reactivity of the ZnO plays an important role in the formation of this interphase. Finally, a clear correlation between the amount of the intermediate valence state and the interphase magnetic properties has been established.

Comparative XANES study on the two electron-doped high-T_c superconductor systems, (Sr,La)CuO_2 and (Nd,Ce)$_2CuO_4$
Y. Tanaka, M. Karppinen, J.M. Chen, R.S. Liu and H. Yamauchi
Page 1217

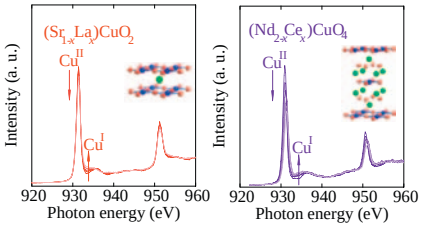

High-quality samples with systematically varied substitution levels of the two electron-doped copper-oxide systems, $(Sr_{1-x}La_x)CuO_2$ and $(Nd_{2-x}Ce_x)CuO_4$, have been synthesized and thoroughly characterized by means of XANES spectroscopy at O-K, Cu-$L_{2,3}$ and Ce-$M_{4,5}$ edges to gain comprehensive understanding of the electronic structure and doping in n-type high-T_c superconductors. Not only common but also slightly different features are revealed for the two systems.

Structure of δ-Bi_2O_3 from density functional theory: A systematic crystallographic analysis
Dilpuneet S. Aidhy, Susan B. Sinnott, Eric D. Wachsman, Simon R. Phillpot and Juan C. Nino
Page 1222

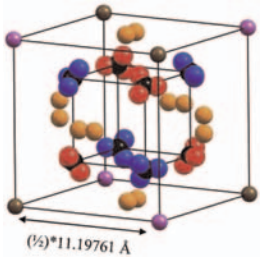

1/8 of a $2 \times 2 \times 2$ δ-Bi_2O_3 superstructure having $Fm\bar{3}$ space group. Every oxygen (black) has three possible positions, only one of which is filled either by O1 (red) or O_2 (blue).

Sol–gel synthesis of nanocomposite materials based on lithium niobate nanocrystals dispersed in a silica glass matrix
Elisa Marenna, Carmela Aruta, Esther Fanelli, Mario Barra, Pasquale Pernice and Antonio Aronne
Page 1229

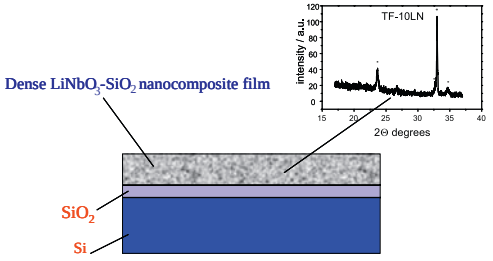

Sol–gel synthesis of nanocomposite materials in the Li_2O–Nb_2O_5–SiO_2 system is reported. The goal was to synthesize thin films containing lithium niobate nanocrystals embedded in a silica matrix. Starting from $LiNO_3$, $NbCl_5$ and $Si(OC_2H_5)_4$, it was possible to obtain $LiNbO_3$ as only crystallizing phase, nanocrystals size was 27 nm for a film $10Li_2O$–$10Nb_2O_5$–$80SiO_2$ heated 2 h at 800 °C.

A general protocol to coat titania shell on carbon-based composite cores using carbon as coupling agent
Rongbo Zheng, Xianwei Meng and Fangqiong Tang
Page 1235

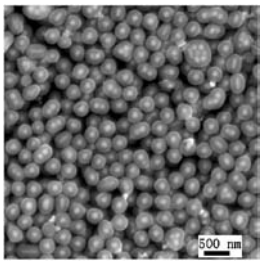

A general protocol was developed to coat titania shell on carbon-based composite cores based on the carbonaceous surface. Typically, Ag/C/TiO_2 core/shell spheres were formed via this method.

Growth of group III nitride films by pulsed electron beam deposition
J. Ohta, K. Sakurada, F.-Y. Shih, A. Kobayashi and H. Fujioka
Page 1241

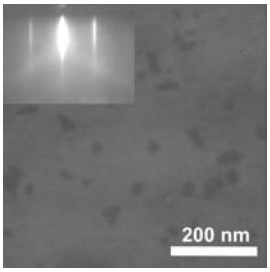

We have grown group III nitride films by pulsed electron beam deposition (PED) and found that the films of group III nitrides grow epitaxially on 6H–SiC and Al_2O_3 substrates. We also found that the use of PED allows us to reduce the epitaxial growth temperature for GaN down to 200 °C.

Syntheses, crystal and electronic structures of three new potassium cadmium(II)/zinc(II) tellurides: $K_2Cd_2Te_3$, K_6CdTe_4 and K_2ZnTe_2
Min-Jie Li, Chun-Li Hu, Xiao-Wu Lei, Yong Zhou and Jiang-Gao Mao
Page 1245

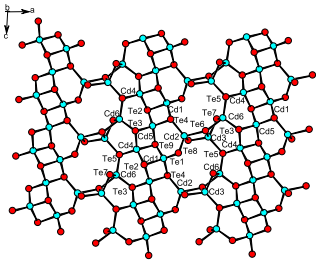

Three new semiconducting K–Zn(Cd)–Te phases were synthesized. They feature 2D, 1D or 0D anionic structure made of corner- and edge-sharing or isolated MTe_4 tetrahedra.

Continued

Determination of the Mössbauer parameters of rare-earth nitroprussides: Evidence for new *l*ight-*i*nduced *m*agnetic *e*xcited *s*tate (*LIMES*) in nitroprussides

V. Rusanov, S. Stankov, A. Ahmedova and A.X. Trautwein

Page 1252

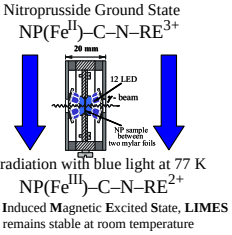

Rare-earth nitroprussides are studied by Mössbauer spectroscopy. Population of metastable states in a thin surface layer, and another state which remains stable at room temperature, are detected. The latter is a photoproduct which is called *l*ight-*i*nduced *m*agnetic *e*xcited *s*tate (*LIMES*) and explained with a photochemical redox reaction, which changes the valence, spin, and magnetic state of 4*f*–3*d* bimetallic complexes.

Synthesis, crystal structure and thermal behavior of a novel oxoborate $SrBi_2B_4O_{10}$

M.G. Krzhizhanovskaya, R.S. Bubnova, A.V. Egorysheva, M.S. Kozin, V.D. Volodin and S.K. Filatov

Page 1260

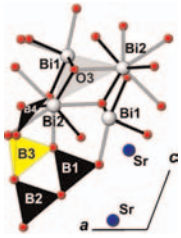

A fragment of $SrBi_2B_4O_{10}$ structure showing isolated borate anion $[B_4O_9]^{6-}$ composed of a triborate group and a triangle, Sr atoms and a part of Bi–O chains involving oxocentred OBi_3 triangles.

Single-crystalline α-Fe_2O_3 with hierarchical structures: Controllable synthesis, formation mechanism and photocatalytic properties

Jianmin Gu, Siheng Li, Enbo Wang, Qiuyu Li, Guoying Sun, Rui Xu and Hong Zhang

Page 1265

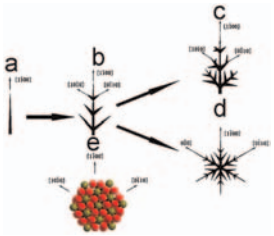

A dual iron precursors system in a hydrothermal process was developed for controllable fabrication of various α-Fe_2O_3 hierarchical structures. Micro-pines, snowflakes and bundles were successfully fabricated by simply tuning the total concentration of the two iron precursors and their molar ratio. A possible formation mechanism of these structures was proposed.

Improvement by heating of the electronic conductivity of cobalt spinel phases, electrochemically synthesized in various electrolytes

Myriam Douin, Liliane Guerlou-Demourgues, Michel Ménétrier, Emilie Bekaert, Lionel Goubault, Patrick Bernard and Claude Delmas

Page 1273

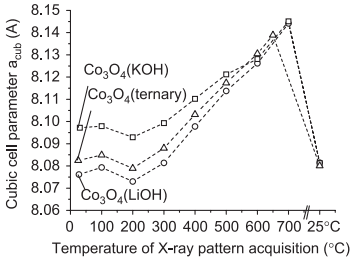

In "Co_3O_4" type spinel phases synthesized by eleectrooxidation, the nature of the alkaline electrolyte allows to monitor the amounts of hydrogen and lithium, inserted in spinel framework and therefore the electronic conductivity. Whatever the initial synthesis electrolyte, a moderate thermal treatment of the materials induces a significant increase of the electronic conductivity, due to a structural reorganization (illustrated by the evolution of the cell parameter) and an increase of the Co^{4+}/Co^{3+} ratio in the octahedral framework.

Corrigendum

Corrigendum to "Solid-state synthesis, characterization and luminescent properties of Eu^{3+}-doped gadolinium tungstate, molybdate phosphors: $Gd_{(2-x)}MO_6:Eu_x^{3+}$ (M = W, Mo)" [Journal of Solid State Chemistry 181 (2008) 2845–2851]

Fang Lei, Bing Yan and Hao-Hong Chen

Page 1281

Author inquiries

For inquiries relating to the submission of articles (including electronic submission where available) please visit this journal's homepage at http://www.elsevier.com/locate/jssc. You can track accepted articles at http://www.elsevier.com/trackarticle and set up e-mail alerts to inform you of when an article's status has changed. Also accessible from here is information on copyright, frequently asked questions and more.
Contact details for questions arising after acceptance of an article, especially those relating to proofs, will be provided by the publisher.

Language services. Authors who require information about language editing and copyediting services pre- and post-submission please visit http://www.elsevier.com/locate/languagepolishing or our customer support site at http://epsupport.elsevier.com. Please note Elsevier neither endorses nor takes responsibility for any products, goods or services offered by outside vendors through our services or in any advertising. For more information please refer to our Terms & Conditions http://www.elsevier.com/termsandconditions

For a full and complete Guide for Authors, please go to: http://www.elsevier.com/locate/jssc

Journal of Solid State Chemistry has no page charges.